THE JOURNAL OF PHYSICAL CHEMISTRY Letters

pubs.acs.org/JPCL Letter

Confronting the Invisible: Assignment of Protein $^{1}H^{N}$ Chemical Shifts in Cases of Extreme Broadening

Leo E. Wong,[‖] Tae Hun Kim, Enrico Rennella, Pramodh Vallurupalli,[‖] and Lewis E. Kay*

Cite This: *J. Phys. Chem. Lett.* 2020, 11, 3384−3389 Read Online

ACCESS | Metrics & More | Article Recommendations | Supporting Information

ABSTRACT: NMR studies of intrinsically disordered proteins (IDPs) at neutral pH values are hampered by the rapid exchange of backbone amide protons with solvent. Although exchange rates can be modulated by changes in pH, interactions between IDPs that lead to phase separation sometimes only occur at neutral pH values or higher, where backbone amide-based experiments fail. Here we describe a simple NMR experiment for measuring amide proton chemical shifts in cases where $^{1}H^{N}$ spectra cannot be obtained. The approach uses a weak ^{1}H B_1 field, searching for elusive $^{1}H^{N}$ resonance frequencies that become encoded in the intensities of cross-peaks in three-dimensional $^{1}H^{\alpha}$-detect spectra. Applications to the CAPRIN1 protein in both dilute- and phase-separated states highlight the utility of the method, establishing that accurate $^{1}H^{N}$ chemical shifts can be obtained even in cases where solvent hydrogen exchange rates are on the order of 1500 s^{-1}.

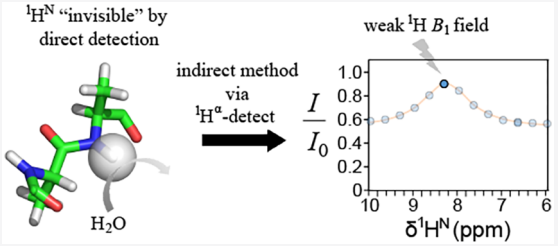

The structure and dynamics of biomolecules are governed by complex energy landscapes, with excursions between minima leading to potentially significant changes in conformation and hence in function.[1,2] The conformers that are produced during this process, often of biological relevance, may only be sparsely populated and transiently formed so that they are invisible to many biophysical methods, including standard solution NMR approaches. The study of these elusive conformers has become possible, however, with the development of spin relaxation-based NMR experiments for their indirect detection[3−5] or via the introduction of perturbants, such as pressure, that can rapidly change their populations to bring them into a window where they can be directly observed.[6] "Seeing the invisible" also becomes of critical importance in applications where signals from highly populated ground states cannot be directly measured. For example, consider the well-known case of rapid solvent hydrogen exchange that leads to broadening and disappearance of labile amide $^{1}H^{N}$ resonances in NMR spectra of proteins. Although in some cases it is possible to lower the pH or temperature to decrease exchange rates so that amide correlations reappear, in other cases this is not feasible, as the system under study may only be stable at pH values greater than neutral and in a prescribed temperature range. In such cases, and especially for intrinsically disordered proteins (IDPs) or intrinsically disordered regions (IDRs) of folded proteins, standard amide proton-detect experiments are likely to fail.

Such a situation is encountered in the study of phase separation when the molecular players only associate at neutral pH or higher. One example is provided by the interaction between CAPRIN1 and FMRP, two highly expressed RNA-binding proteins present in cytoplasmic condensates.[7−10] We have previously shown that the low complexity, intrinsically disordered region of CAPRIN1 (residues 607 to 709, referred to in what follows as CAPRIN1) and the phosphorylated, low-complexity C-terminal region of FMRP (amino acids 452−632) only co-phase separate at pH values close to neutral or above.[7,11] At these pH values, however, the quality of amide-based NMR spectra is very poor (Figures S1 and S2) so that $^{1}H^{N}$ chemical shift assignments are difficult to obtain, as illustrated by the $^{1}H^{N}$-^{15}N correlation spectrum of isolated CAPRIN1 recorded at pH 7.4 (Figure S1). Herein we describe a simple approach for measurement of these elusive chemical shifts, building upon ideas that have emerged for obtaining chemical shifts of nuclei in sparsely populated states of proteins and upon experiments for measuring rapid solvent hydrogen exchange rates in amino acids and proteins.[12−15] Our method shares some features with off-resonance decoupling schemes that have been used to reduce the dimensionality of experiments by calculating chemical shifts from peak splittings;[16−19] however, in the present case rapid solvent hydrogen exchange would preclude such an analysis.

Consider first an isolated $^{1}H^{N}$-^{15}N spin pair. In the absence of solvent exchange, the evolution of ^{15}N magnetization leads to a well-known doublet spectrum with components separated by $^{1}J_{HN}$ (Hz), where $^{1}J_{HN}$ is the one-bond $^{1}H^{N}$-^{15}N scalar

Received: March 6, 2020
Accepted: April 14, 2020
Published: April 14, 2020

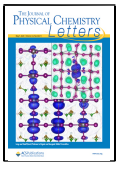

https://dx.doi.org/10.1021/acs.jpclett.0c00747
J. Phys. Chem. Lett. 2020, 11, 3384−3389

coupling constant. Application of a strong ^{1}H decoupling field collapses the ^{15}N doublet, while a weak ^{1}H radio frequency field of strength ν_1 Hz leads to a doublet separation of $J_{\nu 1} = {}^1J_{HN}\Delta/(\nu_1{}^2+\Delta^2)^{0.5}$ (ref 20), where Δ is the offset (Hz) between the position of the decoupling field and the resonance frequency of the $^1H^N$ spin in question. In contrast, when solvent exchange occurs the evolution of ^{15}N magnetization is more complex. Neglecting intrinsic relaxation and for $\nu_1 = 0$ (see Supporting Information)

$$N_y(t) = N_{y,0}e^{-k_{ex}t/2}\left[\cos(\pi J_{eff}t) + \frac{k_{ex}}{2\pi J_{eff}}\sin(\pi J_{eff}t)\right],\ J_{eff} = {}^1J_{HN}\sqrt{(1-\alpha^2)} \quad (1)$$

with $\alpha = k_{ex}/(2\pi|{}^1J_{HN}|)$, and k_{ex} is the rate of solvent exchange. In the case where $\alpha \leq \sim 1$, slow to intermediate exchange, Fourier transformation of eq [1] results in a pair of phase-distorted Lorentzian lines, while in the fast exchange limit ($\alpha \gg 1$) a single Lorentzian line with a width of $k_{ex}/(4\pi\alpha^2)$ is generated (see Supporting Information). In the limit that k_{ex} becomes infinitely fast ($\alpha \rightarrow \infty$) the contribution from exchange to the ^{15}N line width goes to zero, as expected. Note that the exchange time scale in this case is defined relative to the difference in separation between ^{15}N multiplet components, k_{ex} versus $2\pi|{}^1J_{HN}|$. Exchange events, corresponding to the interconversion of multiplet components, occur when an amide proton and a water proton with different spin states exchange; these happen with a frequency of $k_{ex}/2$, and not k_{ex}, since half of the solvent exchange events preserve the spin state of the amide proton.

Building on these simple ideas, we construct the element in Figure 1A, which, in turn, forms the building block in a triple

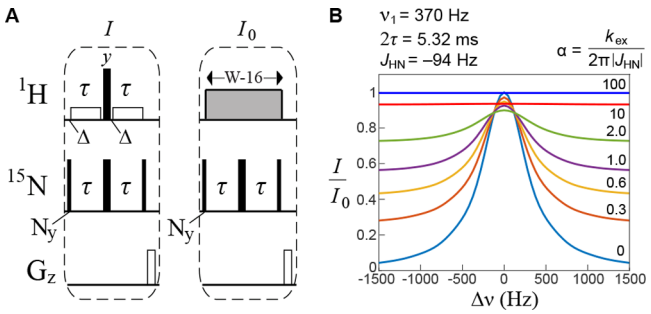

Figure 1. Indirect detection of invisible amide proton resonances. (A) Pulse sequence building block used to establish the resonance positions of invisible amide protons in proteins. The scheme is inserted into the haCONHA triple resonance experiment[11] that allows read-out in a 3D mode by recording ^{13}CO, ^{15}N, and $^1H^\alpha$ chemical shifts (Figure S3). The intensity of in-phase ^{15}N magnetization (I), N_y, is measured at the end of a spin-echo (SE) element of duration 2τ, typically set to an odd multiple of $0.5/{}^1J_{HN}$, with weak ^{1}H irradiation (ν_1) applied at an offset Δ from the unknown $^1H^N$ resonance position; a series of spectra is recorded as a function of Δ. A reference spectrum (I_0) is obtained with high-power ^{1}H WALTZ-16 decoupling (W-16) (~6.25 kHz). (B) Simulated I/I_0 profiles for different α values, as indicated.

resonance pulse scheme that is used to indirectly measure $^1H^N$ chemical shifts (Figure S3). Focusing on Figure 1A and starting from transverse ^{15}N y-magnetization, N_y, we consider a simple spin−echo sequence, with 2τ set to $0.5/{}^1J_{HN}$, and monitor the amount of y-magnetization present at the end of the echo. A series of experiments is recorded, where the position of a relatively weak continuous wave (cw) B_1 field ($\nu_1 \approx 200-500$ Hz), applied continuously during each of the τ delays, is varied across the spectral region of interest, one offset per spectrum (Figure 1A, left). In the absence of solvent hydrogen exchange ($\alpha = 0$), and when the position of the B_1 field is far from the resonance position of the amide proton in question, N_y is completely converted to antiphase x-magnetization during the echo and subsequently eliminated so that no signal is observed ($N_y(2\tau) = 0$). As the B_1 field approaches the amide proton resonance, $J_{\nu 1}$ is decreased (see above), effectively slowing scalar coupled evolution so that a component of y-magnetization remains at the end of the echo, giving rise to observable magnetization. When the B_1 field is on-resonance with the $^1H^N$ spin, $J_{\nu 1} = 0$ Hz, and, neglecting relaxation during the spin−echo, there is no loss in signal from the echo period. The resultant profile is the turquoise curve of Figure 1B, with a maximum at the resonance position of the $^1H^N$ spin (set to 0 Hz in this example). As α increases (i.e., finite solvent exchange), $N_y(2\tau) \neq 0$, even far off-resonance, where the effects of the ^{1}H decoupling field are small, as illustrated in Figure 1B for offsets ($\Delta\nu$) of ±1.5 kHz (see Supporting Information). Although eq [1] does not apply for $\nu_1 \neq 0$, a reasonable approximation for the evolution of N_y can be obtained by substituting $J_{\nu 1}$ for ${}^1J_{HN}$ in eq [1], so long as $\nu_1 > \sim 350$ Hz and $k_{ex} < \sim 200$ s^{-1}. As the B_1 field becomes increasingly close to the resonance position of the ^{1}H spin the effective coupling, $J_{\nu 1}$, is decreased, and a larger component of the detected magnetization, N_y, results. To an excellent approximation, when the B_1 field is on resonance scalar coupled evolution is suppressed, solvent hydrogen exchange therefore no longer contributes to the relaxation of nitrogen magnetization, as there is no buildup of antiphase magnetization, and the intensity of the desired signal (N_y) is a maximum. Figure 1B establishes that, even for $\alpha = 2$, corresponding to $k_{ex} \approx 1200$ s^{-1}, a noticeable maximum in the intensity profile is still observed, suggesting that accurate $^1H^N$ chemical shifts can be obtained at these high exchange rates (verified experimentally below). Notably, as α increases further to values of ~3 and beyond, the profiles become increasingly flat (red and blue curves in Figure 1B), as the effective $^1H^N$-^{15}N coupling is now significantly attenuated, and eventually solvent hydrogen exchange becomes sufficiently rapid so as to lead to a self-decoupling effect with no loss of magnetization during the echo period. In these cases, k_{ex} rates become too large to accurately measure $^1H^N$ chemical shifts using $2\tau = 0.5/{}^1J_{HN}$, $\nu_1 = 370$ Hz. It is thus clear that, although not the primary goal of the experiment in our case, it is also possible to obtain estimates of solvent exchange rates (note the dependence of the offset of the curves as a function of α in Figure 1B). Indeed, Pelupessy and co-workers have developed related experiments for measuring ultrafast solvent exchange rates for $^1H^N$ protons in side chains of amino acids and proteins (~10^5 s^{-1}),[12−14] and Dass et al. have extended this approach to applications involving backbone amides in proteins.[15] As a final note, an additional experiment is recorded with a strong ^{1}H decoupling field applied during the complete echo period (Figure 1A, right). The ratio of intensities I/I_0 as a function of $\Delta\nu$ (Figure 1B) thus produces a plot extending from 0 to 1 in this case, where intrinsic relaxation during the scheme is canceled out. The above discussion is qualitative. Exact profiles of I/I_0 can be generated by considering the evolution of $\{N_y, 2N_xH_z, 2N_xH_x, 2N_xH_y\}$ resulting from scalar coupling, solvent hydrogen exchange, and the application of a ^{1}H B_1 field of strength ν_1 (see Supporting

https://dx.doi.org/10.1021/acs.jpclett.0c00747
J. Phys. Chem. Lett. 2020, 11, 3384−3389

Information), where A_j is the j component of A magnetization.[12]

The proposed experiment borrows ideas from chemical exchange saturation transfer (CEST),[21] where a field is swept, one frequency at a time, in search of a maximum perturbation to the intensity of the observed major state correlation that occurs when the B_1 field is on-resonance with the corresponding spin in the excited state.[5] For the application described here, the field is swept so as to maximize the signal intensity. This occurs when the position of the B_1 field is coincident with the resonance frequency of the $^1H^N$ spin in the ground state, allowing its chemical shift to be obtained even if the peak itself cannot be observed.

The pulse scheme that has been developed for the measurement of $^1H^N$ chemical shifts in cases where $^1H^N$-^{15}N correlations are not observed in heteronuclear single quantum coherence spectroscopy (HSQC) spectra is illustrated in Figure S3 and described succinctly by the following magnetization transfer scheme

$$^1H^{\alpha} \xrightarrow{J_{HC}} {}^{13}C^{\alpha} \xrightarrow{J_{CaCO}} {}^{13}CO(t_1) \xrightarrow{J_{NCO}} {}^{15}N(t_2) \xrightarrow{J_{NCO}} {}^{13}CO \xrightarrow{J_{CaCO}} {}^{13}C^{\alpha} \xrightarrow{J_{HC}} {}^1H^{\alpha}(t_3)$$

where the active couplings are indicated above each arrow, and t_i denotes an acquisition time. The spin−echo element of Figure 1A is inserted immediately after ^{15}N chemical shift evolution (t_2) so that the resultant intensities of (^{13}CO, ^{15}N, $^1H^{\alpha}$) correlations, linking ^{13}CO and $^1H^{\alpha}$ chemical shifts of residue j with the ^{15}N shift of residue j+1, are modulated in the manner shown in Figure 1B. This experiment is closely related to an haCONHA scheme that was recently proposed as part of a suite of pulse sequences for backbone assignment of intrinsically disordered proteins,[11] and we refer to the experiment here as SE_haCONHA, to denote the fact that a spin−echo (SE) is inserted that enables the indirect measurement of $^1H^N$ shifts.

To validate the methodology, we first applied our approach to a sample of CAPRIN1 that is not phase-separated (referred to as a dilute sample in what follows). Under the conditions of our experiment (pH 5.5, 25 °C) high-quality HNCO data sets can be recorded so that the $^1H^N$ chemical shifts measured directly can be compared with those obtained indirectly using the SE_haCONHA method. Nineteen three-dimensional (3D) SE_haCONHA data sets of CAPRIN1 were measured, with the weak ^1H B_1 field (392 Hz) separated by 150 Hz in each spectrum so as to span the range of possible $^1H^N$ chemical shifts (Table S1). To minimize the net measurement time, we used nonuniform sampling in the indirect dimensions[22−24] and then fit the time domain directly, after Fourier transformation of the direct detect dimension, using a procedure described previously[25] and discussed in the Supporting Information. The resultant I/I_0 profiles were found to be more accurate than the corresponding curves generated from fits of frequency domain data. Figure 2A illustrates typical profiles obtained for four residues in CAPRIN1 (blue circles) and the corresponding fits (orange curves) that take into account the scalar coupled and chemical shift evolution of ^{15}N magnetization during the spin−echo period of Figure 1A, as well as the effects of solvent hydrogen exchange (see Supporting Information). A linear correlation plot of $^1H^N$ chemical shifts measured either from HNCO or SE_haCONHA data sets is shown in Figure 2B, with excellent agreement obtained. Notably, we obtained $^1H^N$

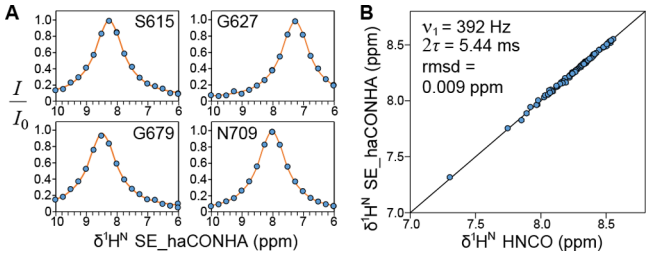

Figure 2. Accurate determination of $^1H^N$ chemical shifts from SE_haCONHA data. (A) Representative experimental data (blue circles) and best-fit curves (orange lines) from measurements recorded on a dilute-phase CAPRIN1 sample (0.5 mM) dissolved in 25 mM 2-(*N*-morpholino)ethanesulfonic acid (MES) buffer, pH 5.5, 25 °C. Under these conditions $^1H^N$ chemical shifts can be measured in an HNCO experiment for validation. (B) Linear correlation plot of $^1H^N$ chemical shifts as measured in a 3D HNCO data set or determined from fits of SE_haCONHA data (parameters listed in inset). Error bars in (A, B) are smaller than symbols.

shifts for all residues in CAPRIN1 (pH 5.5) using our new approach. Consistent with the results of Figure 2B, we established that the small variation in $^1J_{HN}$ values in proteins (−93.7 ± 1.1 Hz for maltose binding protein[26] and between −94.2 and −93.0 Hz in the unfolded protein Tau[27]) has no influence on extracted $^1H^N$ chemical shifts and only small effects on measured solvent hydrogen exchange rates (see below), Figure S4.

Having validated the method, we next recorded experiments on a dilute CAPRIN1 sample at pH 7.4 (25 mM 4-(2-hydroxyethyl)-1-piperazineethanesulfonic acid (HEPES)) and 30 °C, where the solvent exchange rates were much higher, and the quality of $^1H^N$-^{15}N-based spectra very significantly reduced (Figures S1 and S2). Data were recorded for a pair of τ values, $2\tau \approx 0.5/^1J_{HN}$, $1.5/^1J_{HN}$, and at three ^1H B_1 fields, ν_1 = 196, 392, and 530 Hz. Figure 3A,C shows profiles obtained for a pair of residues with high and low k_{ex} rates (S615, k_{ex} = 1500 ± 40 s^{-1}; G627, k_{ex} = 85 ± 5 s^{-1}) using different τ and ν_1 values, as indicated. As expected for amides with large k_{ex} rates, the peak for S615 is broad, and the baseline is elevated (see Figure 1B); better dynamic range can be obtained by using a longer 2τ value and a stronger ^1H ν_1, as shown. In this context, as long as sensitivity is not limiting, $2\tau \approx 1.5/^1J_{HN}$ is preferred over $0.5/^1J_{HN}$, as errors in extracted parameters are smaller. It is of interest to note how the baseline for G627 ($\alpha \approx 0.15$) changes with ^1H B_1 field offset for the case where $2\tau \approx 1.5/^1J_{HN}$. This can be understood most easily in the limit where k_{ex} = 0 s^{-1}, in which case the intensity profile is reasonably approximated by $\cos(\theta)$, where $\theta = 2\pi J_{\nu 1}\tau = 1.5\pi\, J_{\nu 1}/^1J_{HN}$, with θ varying from 1.5π (^1H B_1 field far off resonance) to 0 (on resonance). In contrast, when $2\tau \approx 0.5/^1J_{HN}$, θ ranges from 0.5π to 0, and $\cos(\theta)$ is always non-negative. Figure 3B,D presents correlation plots of extracted $^1H^N$ chemical shifts or k_{ex} values, with excellent agreement noted between the different experiments, and the level of agreement did not degrade when only ∼50% of the data were analyzed to extract parameters (Figure S5). In comparison to an HNCO data set for measuring $^1H^N$ chemical shifts, recorded on the same sample and under the same conditions, the SE_haCONHA approach is superior, yielding 87 shifts relative to 48 for the HNCO out of a total of 92 amide protons in CAPRIN1. It is noteworthy that the HNCO was optimized using an approach previously described for

https://dx.doi.org/10.1021/acs.jpclett.0c00747
J. Phys. Chem. Lett. 2020, 11, 3384−3389

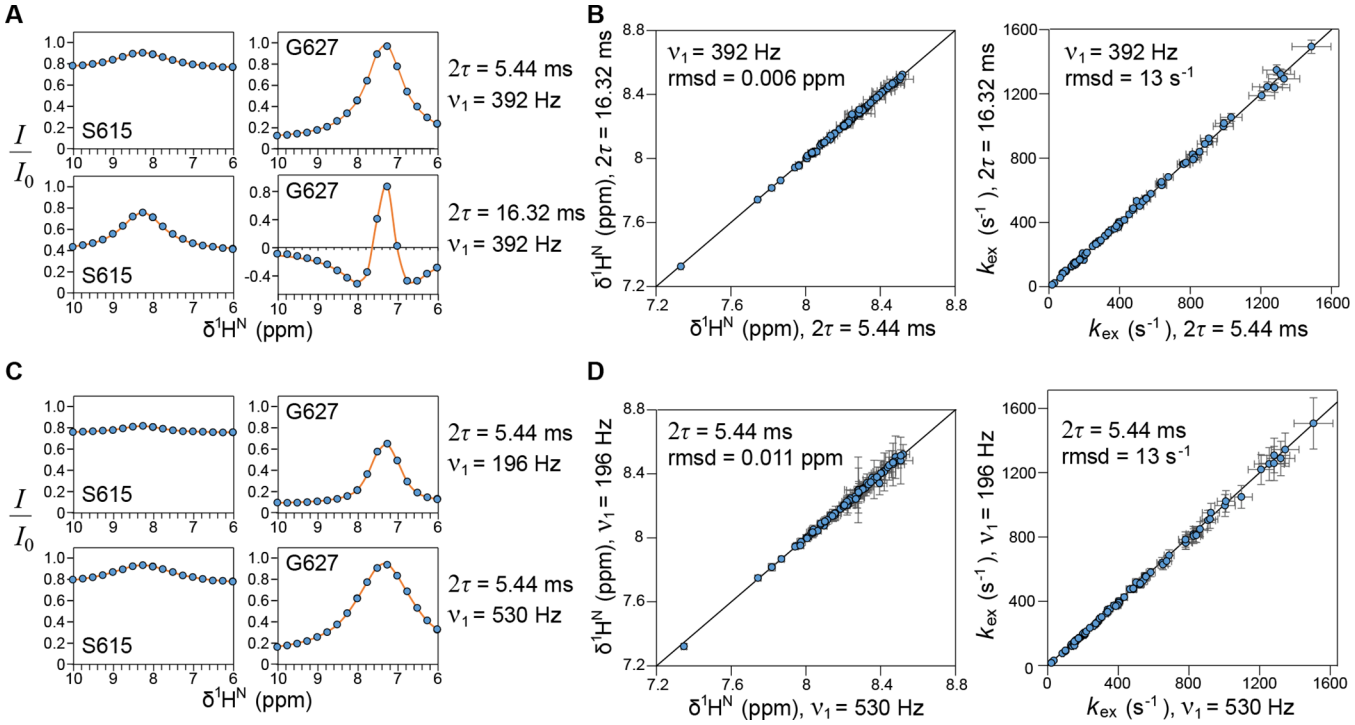

Figure 3. Robust fits of $^{1}H^{N}$ chemical shifts and k_{ex}. (A, C) I/I_0 profiles (blue circles) and best-fit curves (orange lines) are shown for residues S615 and G627 of CAPRIN1 (dilute phase sample, 25 mM HEPES buffer, pH 7.4, 30 °C; only poor-quality HNCO spectra can be recorded under these conditions). The data were acquired with the SE_haCONHA scheme of Figure S3 using different experimental parameters, as indicated to the right of the panels. (B, D) Linear correlation plots of extracted $^{1}H^{N}$ chemical shift or k_{ex} values fit from SE_haCONHA spectra recorded with different parameters, as indicated. The larger errors in the parameters for amides with downfield $^{1}H^{N}$ shifts correlate with higher water exchange rates.

recording HSQC data sets of unfolded proteins,[28] where exchange of amide proton magnetization with water in the initial polarization transfer from $^{1}H^{N}$ to ^{15}N increases the sensitivity of the experiment. Of the five $^{1}H^{N}$ shifts that could not be obtained from analysis of the 3D SE_haCONHA data, two are due to peak overlap, two peaks, derived from IsoAsp-Gly linkages,[11] are eliminated by $^{13}C^{\beta}$ decoupling (see Figure S3), with k_{ex} too large to obtain reliable fits for the remaining amide (R608). Notably, when a set of two-dimensional (2D) $^{15}N-^{1}H^{\alpha}$ planes (Figure S3) was recorded with $2\tau \approx 2.5/^{1}J_{HN}$ and ν_1 = 1960 Hz, it was possible to measure both the $^{1}H^{N}$ chemical shift and $k_{ex} = 7100 \pm 700\ s^{-1}$ for this residue (Figure S6).

A set of comparative experiments, as in Figure 2, was also performed on a sample of the condensed phase of CAPRIN1 (25 mM sodium phosphate, 100 mM NaCl, pH 7.4, 40 °C), prepared as described previously.[11] The large concentration of protein in the phase-separated state (~15 mM) challenges the measurements, because the high sample viscosity leads to a significant reduction in spectral sensitivity. We were able to obtain 65 and 55 $^{1}H^{N}$ shifts from the SE_haCONHA and HNCO experiments, respectively, recorded with the same measurement times, with 26 chemical shifts unique to the SE_haCONHA experiment. Notably, the same 65 shifts could be measured robustly when successive frequency points were excluded from the analysis (Figure S5). Figure 4A highlights profiles from residues S615 and G679 of CAPRIN1 recorded with $2\tau \approx 0.5/^{1}J_{HN}$ and ν_1 = 392 Hz. Extracted $^{1}H^{N}$ chemical shifts from HNCO (blue circles) and SE_haCONHA profiles (open circles) are plotted in Figure 4B as a function of residue number. Both experiments are complementary in that amide proton shifts for some residues in one experiment are

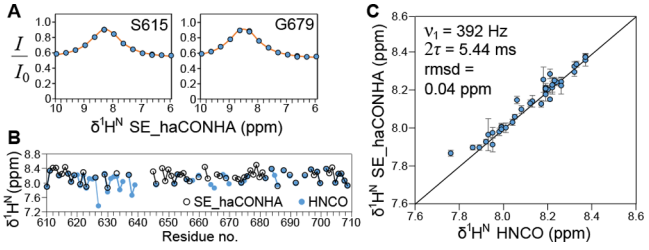

Figure 4. An application to a condensed-phase CAPRIN1 sample. (A) Experimental I/I_0 profiles (blue circles) and best-fit curves (orange lines) for S615 and G679 of CAPRIN1 (condensed phase sample, ~15 mM protein of which ~2 mM is ^{13}C,^{15}N-labeled, 25 mM sodium phosphate, 100 mM NaCl, pH 7.4, 40 °C). (B) Plot of $^{1}H^{N}$ shifts, as measured from SE_haCONHA (65 residues, open circles; ν_1 = 392 Hz, 2τ = 5.44 ms) or from peak positions in an HNCO data set (55 residues, blue circles). (C) Linear correlation plot of the common set of $^{1}H^{N}$ shifts in (B).

sometimes not observed in the second; in total 81 chemical shifts were obtained. $^{1}H^{N}$ shifts that were available from both experiments are shown in the linear correlation plot of Figure 4C, establishing that, even for condensed-phase samples, reasonably accurate chemical shift values can be measured. Figure S7 plots $^{1}H^{N}$ chemical shifts for dilute and phase-separated CAPRIN1 samples, showing only small differences. The $^{1}H^{N}$ resonances of a number of Gly residues are noticeably upfield shifted (Table S2), suggesting that CAPRIN1 is not a complete random coil. Notably, for these glycines other backbone nuclei do not show chemical shift perturbations. The importance of amide proton chemical shifts as structural probes, in general, is made clear by the fact that $^{1}H^{N}$ and other backbone chemical shifts are powerful reporters

https://dx.doi.org/10.1021/acs.jpclett.0c00747
J. Phys. Chem. Lett. 2020, 11, 3384−3389

of secondary structure, $^{1}H^{N}$ chemical shifts are sensitive to hydrogen bond lengths, and their temperature dependencies are indicators of hydrogen bonding.[29−32]

In summary, we have described an approach for obtaining amide proton chemical shifts, using an indirect method in which intensities of correlations in an $^{1}H^{\alpha}$-based triple resonance scheme are modulated by a weak ^{1}H B_1 field that "searches" across the $^{1}H^{N}$ spectral region for the chemical shifts of interest. The experiment fills an important void in providing $^{1}H^{N}$ chemical shift assignments for disordered proteins or disordered regions of folded proteins, in either dilute or condensed phases, in cases where solvent hydrogen exchange rates are sufficiently rapid to preclude the recording of high-quality $^{1}H^{N}$-^{15}N correlations.

■ ASSOCIATED CONTENT

Supporting Information

The Supporting Information is available free of charge at https://pubs.acs.org/doi/10.1021/acs.jpclett.0c00747.

Materials and methods, derivation of eq [1], description of time-domain data analysis, figures, tables, and pulse sequence of the SE_haCONHA experiment (PDF)

■ AUTHOR INFORMATION

Corresponding Author

Lewis E. Kay − *Departments of Molecular Genetics, Biochemistry and Chemistry, University of Toronto, Toronto, Ontario M5S 1A8, Canada; Program in Molecular Medicine, Hospital for Sick Children, Toronto, Ontario M5G 1X8, Canada;* orcid.org/0000-0002-4054-4083; Email: kay@pound.med.utoronto.ca

Authors

Leo E. Wong − *Departments of Molecular Genetics, Biochemistry and Chemistry, University of Toronto, Toronto, Ontario M5S 1A8, Canada*

Tae Hun Kim − *Program in Molecular Medicine, Hospital for Sick Children, Toronto, Ontario M5G 1X8, Canada*

Enrico Rennella − *Departments of Molecular Genetics, Biochemistry and Chemistry, University of Toronto, Toronto, Ontario M5S 1A8, Canada;* orcid.org/0000-0002-2941-7155

Pramodh Vallurupalli − *TIFR Centre for Interdisciplinary Sciences, Tata Institute of Fundamental Research Hyderabad, Hyderabad, Telangana 500107, India;* orcid.org/0000-0002-0936-6098

Complete contact information is available at: https://pubs.acs.org/10.1021/acs.jpclett.0c00747

Author Contributions

‖These authors contributed equally to this work.

Notes

The authors declare no competing financial interest.

■ ACKNOWLEDGMENTS

This work was supported by grants from the Natural Sciences and Engineering Research Council of Canada and the Canadian Institutes of Health Research (CIHR) to L.E.K. and by funds from TCIS/TIFRH to P.V. T.H.K. is grateful for support in the form of a Banting postdoctoral fellowship from the CIHR. L.E.K. holds a Canada Research Chair in Biochemistry.

■ REFERENCES

(1) Karplus, M.; Kuriyan, J. Molecular Dynamics and Protein Function. *Proc. Natl. Acad. Sci. U. S. A.* **2005**, *102* (19), 6679−6685.

(2) Sekhar, A.; Kay, L. E. An NMR View of Protein Dynamics in Health and Disease. *Annu. Rev. Biophys.* **2019**, *48*, 297−319.

(3) Palmer, A. G.; Kroenke, C. D.; Loria, J. P. Nuclear Magnetic Resonance Methods for Quantifying Microsecond-to-Millisecond Motions in Biological Macromolecules. In *Methods in Enzymology;* 2001; pp 204−238. DOI: 10.1016/S0076-6879(01)39315-1.

(4) Anthis, N. J.; Clore, G. M. Visualizing Transient Dark States by NMR Spectroscopy. *Q. Rev. Biophys.* **2015**, *48* (1), 35−116.

(5) Vallurupalli, P.; Bouvignies, G.; Kay, L. E. Studying "Invisible" Excited Protein States in Slow Exchange with a Major State Conformation. *J. Am. Chem. Soc.* **2012**, *134* (19), 8148−8161.

(6) Charlier, C.; Alderson, T. R.; Courtney, J. M.; Ying, J.; Anfinrud, P.; Bax, A. Study of Protein Folding under Native Conditions by Rapidly Switching the Hydrostatic Pressure inside an NMR Sample Cell. *Proc. Natl. Acad. Sci. U. S. A.* **2018**, *115* (18), E4169−E4178.

(7) Kim, T. H.; Tsang, B.; Vernon, R. M.; Sonenberg, N.; Kay, L. E.; Forman-Kay, J. D. Phospho-Dependent Phase Separation of FMRP and CAPRIN1 Recapitulates Regulation of Translation and Deadenylation. *Science* **2019**, *365* (6455), 825−829.

(8) Tsang, B.; Arsenault, J.; Vernon, R. M.; Lin, H.; Sonenberg, N.; Wang, L. Y.; Bah, A.; Forman-Kay, J. D. Phosphoregulated FMRP Phase Separation Models Activity-Dependent Translation through Bidirectional Control of MRNA Granule Formation. *Proc. Natl. Acad. Sci. U. S. A.* **2019**, *116* (10), 4218−4227.

(9) Youn, J. Y.; Dunham, W. H.; Hong, S. J.; Knight, J. D. R.; Bashkurov, M.; Chen, G. I.; Bagci, H.; Rathod, B.; MacLeod, G.; Eng, S. W. M.; et al. High-Density Proximity Mapping Reveals the Subcellular Organization of MRNA-Associated Granules and Bodies. *Mol. Cell* **2018**, *69* (3), 517−532.

(10) El Fatimy, R.; Tremblay, S.; Dury, A. Y.; Solomon, S.; de Koninck, P.; Schrader, J. W.; Khandjian, E. W. Fragile Mental Retardation Protein Interacts with the RNA-Binding Protein Caprin1 in Neuronal Ribonucleoprotein Complexes. *PLoS One* **2012**, *7* (6), No. e39338.

(11) Wong, L. E.; Kim, T. H.; Muhandiram, D. R.; Forman-Kay, J. D.; Kay, L. E. NMR Experiments for Studies of Dilute and Condensed Protein Phases: Application to the Phase-Separating Protein CAPRIN1. *J. Am. Chem. Soc.* **2020**, *142*, 2471.

(12) Kateb, F.; Pelupessy, P.; Bodenhausen, G. Measuring Fast Hydrogen Exchange Rates by NMR Spectroscopy. *J. Magn. Reson.* **2007**, *184* (1), 108−113.

(13) Segawa, T.; Kateb, F.; Duma, L.; Bodenhausen, G.; Pelupessy, P. Exchange Rate Constants of Invisible Protons in Proteins Determined by NMR Spectroscopy. *ChemBioChem* **2008**, *9* (4), 537−542.

(14) Sehgal, A. A.; Duma, L.; Bodenhausen, G.; Pelupessy, P. Fast Proton Exchange in Histidine: Measurement of Rate Constants through Indirect Detection by NMR Spectroscopy. *Chem. - Eur. J.* **2014**, *20* (21), 6332−6338.

(15) Dass, R.; Corlianò, E.; Mulder, F. A. A. Measurement of Very Fast Exchange Rates of Individual Amide Protons in Proteins by NMR Spectroscopy. *ChemPhysChem* **2019**, *20* (2), 231−235.

(16) Fesik, S. W.; Eaton, H. L.; Olejniczak, E. T.; Gampe, R. T. Pseudo-Four-Dimensional Nuclear Magnetic Resonance by Off-Resonance Decoupling. An Approach for Distinguishing Coupled Proton Pairs by the Frequencies of Their Attached Heteronuclei. *J. Am. Chem. Soc.* **1990**, *112* (13), 5370−5371.

(17) Grace, C. R. R.; Riek, R. Pseudomultidimensional NMR by Spin-State Selective Off-Resonance Decoupling. *J. Am. Chem. Soc.* **2003**, *125* (51), 16104−16113.

(18) Keller, R.; Grace, C. R. R.; Riek, R. Fast Multidimensional NMR Spectroscopy by Spin-State Selective off-Resonance Decoupling (SITAR). *Magn. Reson. Chem.* **2006**, *44* (S1), S196−S205.

(19) Bouvignies, G.; Kay, L. E. Measurement of Proton Chemical Shifts in Invisible States of Slowly Exchanging Protein Systems by

Chemical Exchange Saturation Transfer. *J. Phys. Chem. B* **2012**, *116* (49), 14311−14317.
(20) Freeman, R. *A Handbook of Nuclear Magnetic Resonance,* 1st ed.; Wiley, 1987.
(21) Forsén, S.; Hoffman, R. A. Study of Moderately Rapid Chemical Exchange Reactions by Means of Nuclear Magnetic Double Resonance. *J. Chem. Phys.* **1963**, *39* (11), 2892−2901.
(22) Jaravine, V.; Ibraghimov, I.; Yu Orekhov, V. Removal of a Time Barrier for High-Resolution Multidimensional NMR Spectroscopy. *Nat. Methods* **2006**, *3* (8), 605−607.
(23) Stanek, J.; Koźmiński, W. Iterative Algorithm of Discrete Fourier Transform for Processing Randomly Sampled NMR Data Sets. *J. Biomol. NMR* **2010**, *47* (1), 65−77.
(24) Hyberts, S. G.; Arthanari, H.; Wagner, G. *Applications of Non-Uniform Sampling and Processing;* Billeter, M., Orekhov, V., Eds.; Springer: Berlin, Germany, 2012; Vol. *316*. DOI: 10.1007/128_2011_187.
(25) Long, D.; Delaglio, F.; Sekhar, A.; Kay, L. E. Probing Invisible, Excited Protein States by Non-Uniformly Sampled Pseudo-4D CEST Spectroscopy. *Angew. Chem., Int. Ed.* **2015**, *54* (36), 10507−10511.
(26) Yang, D.; Venters, R. A.; Mueller, G. A.; Choy, W. Y.; Kay, L. E. TROSY-Based HNCO Pulse Sequences for the Measurement of (1)HN-(15)N, (15)N-(13)CO, (1)HN-(13)CO, (13)CO-(13)C(α) and (1)HN-(13)C(α) Dipolar Couplings in (15)N, (13)C, (2)H-Labeled Proteins. *J. Biomol. NMR* **1999**, *14* (4), 333−343.
(27) Xiang, S. Q.; Narayanan, R. L.; Becker, S.; Zweckstetter, M. N-H Spin-Spin Couplings: Probing Hydrogen Bonds in Proteins. *Angew. Chem., Int. Ed.* **2013**, *52* (12), 3525−3528.
(28) Yuwen, T.; Skrynnikov, N. R. CP-HISQC: A Better Version of HSQC Experiment for Intrinsically Disordered Proteins under Physiological Conditions. *J. Biomol. NMR* **2014**, *58* (3), 175−192.
(29) Ohnishi, M.; Urry, D. W. Temperature Dependence of Amide Proton Chemical Shifts: The Secondary Structures of Gramicidin S and Valinomycin. *Biochem. Biophys. Res. Commun.* **1969**, *36* (2), 194−202.
(30) Wishart, D. S.; Sykes, B. D.; Richards, F. M. Relationship between Nuclear Magnetic Resonance Chemical Shift and Protein Secondary Structure. *J. Mol. Biol.* **1991**, *222* (2), 311−333.
(31) Pardi, A.; Wagner, G.; Wüthrich, K. Protein Conformation and Proton Nuclear-magnetic-resonance Chemical Shifts. *Eur. J. Biochem.* **1983**, *137* (3), 445−454.
(32) Asakura, T.; Taoka, K.; Demura, M.; Williamson, M. P. The Relationship between Amide Proton Chemical Shifts and Secondary Structure in Proteins. *J. Biomol. NMR* **1995**, *6* (3), 227−236.

https://dx.doi.org/10.1021/acs.jpclett.0c00747
J. Phys. Chem. Lett. 2020, 11, 3384−3389